

Improved Electrochemical Properties of Cu-doped $\text{LaNi}_{4.1-x}\text{Co}_{0.6}\text{Mn}_{0.3}\text{Cu}_x$ ($x= 0-0.45$) Hydrogen Storage Alloys at 238 K

Chengyuan Ni¹, Zhaozhong Zhou¹, Dongdong Zhu^{1,*}, Zhongmin Wang², Defeng Zhang¹,
Yuanxiang Zhang¹

¹ School of Mechanical Engineering, Quzhou University, Quzhou, Zhejiang 324000, China

² School of Materials Science and Engineering, Guilin University of Electronic Technology, Guilin,
Guangxi 541004, China

*E-mail: zhudd8@hotmail.com

Received: 23 September 2014 / Accepted: 19 October 2014 / Published: 17 November 2014

The effects of Cu content and temperature on the hydrogen storage properties, including gaseous phase hydrogen storage and electrochemical performances were investigated, and the improved low-temperature properties of Cu-doped $\text{LaNi}_{4.1-x}\text{Co}_{0.6}\text{Mn}_{0.3}\text{Cu}_x$ ($x= 0-0.45$) alloys at 238K were intensively discussed. Cu prefers to occupy the 2c site in these alloys, which enlarges the volume of unit cell, lowers the c/a ratios and flattens the pressure-concentration-temperature (PCT) isotherm. The incorporation of Cu, decrease obviously the maximum and reversible hydrogen storage capacity, as well as the desorption pressure and PCT hysteresis. Meanwhile, the maximum hydrogen storage capacities decrease, whereas the reversible hydrogen storage capacities increase at elevated temperature, resulting in increase of reversible capacity ratio. All the alloy electrodes show high dischargeabilities above 300 mAh/g, and good high-rate recoverability properties at 238K. The electrochemical capacity at low temperature is determined by the hydrogen absorption capacity and charge efficiency. In addition, the amount of Cu-content $x=0.15$ is recommended for the nickel/metal hydride battery used in terms of the maximum and high-rate dischargecapacity, and catalytic properties of the alloy electrodes at a temperature as low as 238K. The addition of Cu improves the electrocatalytic activity, but decreases the hydrogen diffusion (D_H) monotonously, indicating that the decrease in HRD at 303K is owing to the lower D_H with Cu-substitution. Since the activation energy of hydrogen diffusion is significantly lower than kinetically controlled reactions, the hydrogen diffusion in the bulk is supposed not to be influenced appreciably at low temperature. Therefore the charge-transfer reaction on the electrode surface is the rate-determining step in the charge process of the negative electrode at 238K was. The improvement in surface reactivity must be essential for improving the electrochemical performance at 238K.

Keywords: Hydrogen storage alloy; Pressure-composition isotherms; Low temperature property; High-rate recoverability; Electrochemical kinetics

1. INTRODUCTION

Rare earth-based AB₅-type hydrogen storage alloys have been studied and applied extensively for metal-hydrogen system [1-3], and are still one of the most important choices in commercial nickel/metal hydride battery (Ni/MH) industry because of its various advantages [4-7], including high power density, resistance to overcharge and long cycle life. However, the Ni/MH batteries have to show a stable performance at a temperature as low as 233 K in order to replace Ni-Cd battery that works in military devices and gelid areas. Nowadays, the discharge performance of commercial AB₅-type alloy electrodes at low temperature, however, is poor and the general operating temperature with decent performance is limited to above 253 K [8]. As a result, the research and development of high-power type Ni/MH battery for low-temperature situation has become imperative [9-12].

Elemental substitution on either A-site or B-site is regarded as an effective way of improving the overall properties of hydrogen storage alloys in order to obtain desired properties. On the one hand, the partial substitution of A-site La by Ce or Nd in rare earth-based AB₅-type alloys improves markedly the hydrogen diffusion rate in the bulk and charge transfer rate on the surface, as well as the low temperature dischargeability [13-17]. On the other hand, the partial substitution of Ni on the B-site by elements, such as Al, Mn, Mo and Fe, is also beneficial to the AB₅-type hydrogen storage alloys in terms of low temperature properties [18-20]. The partial substitution of Ni with Mo reduces charge transfer resistance and increases double layer capacitance in the Mo-containing alloys, which results in an enhanced the low temperature capacity [21]. Fe is also used to replace Ni and beneficial to the charge and discharge efficiency of the electrodes at low temperatures [22-23]. Another transition metal, Cu, with the similar electronegativity and atom radius as Ni and Co, exhibits similar effects as Co in suppressing the pulverization rate [18, 24]. Cu may be an interesting candidate for low-temperature applications because it modifies the surface oxide by filling it with voids, tunnels, and metallic scrolls instead of regular granular shapes for the Cu-modified AB₅ alloys to achieve improved low-temperature electrochemical performance at 263K [25]. However, the study on the low temperature electrochemical performance of Cu-contain alloy worked as low as 238K, to the best of the authors' knowledge, has rarely been seen in literature.

In our previous study, the microstructure and electrochemical properties of LaNi_{4.1-x}Co_{0.6}Mn_{0.3}Cu_x (x= 0-0.45) hydrogen storage alloys at room temperature has been studied [26]. The four alloy electrodes present good activation property and higher capacity, which are suitable for electrochemical application as MH negative electrodes. In this study, the effects of Cu content and temperature on the hydrogen storage properties, including gaseous phase hydrogen storage and electrochemical performances were discussed. Accordingly, the improved low-temperature properties of Cu-dopped LaNi_{4.1-x}Co_{0.6}Mn_{0.3}Cu_x (x= 0-0.45) alloys at 238K were also presented in this paper.

2. EXPERIMENTAL

2.1 Synthesis, characterization, and gaseous study

The alloys with composition LaNi_{4.1-x}Co_{0.6}Mn_{0.3}Cu_x (x=0-0.45) were synthesized in an inductive furnace under argon atmosphere and ground to powders below 250 mesh. The X-ray

diffraction (XRD) analysis was carried out using a D8 ADVANCED (Cu- $K\alpha$ radiation) X-ray diffraction, and the phase distribution and composition was characterized by scanning electron microscopy (SEM). The lattice parameters and cell volumes were analyzed by the Materials Data Inc. software Jade 5.0 and a Power Diffraction File (PDF release 2004). Before the test of cycled morphology, the alloy particles after electrochemical testing were purged in alcohol for several times. PCT characteristics for each sample were measured using a Seiverts-type PCT analysis system (Setaram PCTPro2000), and the PCT isotherms were obtained in the temperature range 303-353K and the pressure range 0.001-0.5 MPa.

2.2 Electrochemical measurement

Details of the fabrication of testing battery have been reported in previously [27]. After being activated at 303 K, the low-temperature properties of the batteries were tested in a cooling system. In order to fully activated at 238K, each sample electrode was charge at a low current density of 30 mA/g for 5 cycles, then the discharge current varied to 60 mA/g. A 2h conservation at 238K prior to the test was used to ensure the discharge temperature of test batteries and the temperature of KOH electrolyte. To evaluate the low-temperature properties, the discharge current varies from 30 mA/g to 300 mA/g and the obtained discharge capacity is denoted as $C_{i,238}$.

Electrochemical impedance spectroscopy (*EIS*) was carried out after the electrodes were fully activated using a Modulab Electrochemical System of Solartron Analytical. The electrode was charged to a depth of discharge (*DOD*) of 50% at 60 mA/g, and then the *EIS* of the electrode was measured using an AC since perturbation of 5 mV in the frequency range of 1 mHz to 100 kHz. The linear polarization curves were measured by scanning electrode potential at the rate 0.1 mV/s from -5 to 5 mV (vs. open circuit potential) at 50% depth of discharge. As for the potential static step discharge, the electrodes were in fully charged state, and discharged at +500 mV potential steps for 3000 s on the same Modulab electrochemical system.

3. RESULTS AND DISCUSSION

3.1 Crystal structure analysis

Fig. 1 shows the XRD spectra of $\text{LaNi}_{4.1-x}\text{Co}_{0.6}\text{Mn}_{0.3}\text{Cu}_x$ ($x=0, 0.15, 0.3, 0.45$) hydrogen storage alloys. All the major peaks can be fit into a hexagonal CaCu_5 crystal structure without any observable impurity. The lattice constants of the four alloys, calculated from the XRD patterns are listed in Table 1. As the amount of Cu increase, both lattice constant and cell volume of the alloys increase monotonically. The cell volume increases from 87.37 in $x=0$ to 88.39 \AA^3 in $x=0.45$. However, the value of c increases slightly, resulting in the decrease of c/a . Although the atomic radius of Cu (1.45 \AA) is slightly smaller than that of Ni (1.49 \AA), the 12-coordinate metallic radius of Cu (1.278 \AA) is actually larger than that of Ni (1.246 \AA). Hence, the high Cu-content increases the lattice constants, suggesting that the Cu-containing metal hydride (MH) has stronger metal-hydrogen (M-H) bond

strength and consequently a lower equilibrium plateau pressure. The decrease of c/a can be explained by preferential Cu-occupancy sites in LaNi_5 crystal structure. Compared to Ni, the not-as-large Cu has a slight preference to occupy the 2c site over the 3g site as Al, Fe, Mn stayed [28]. It is possible that the additional Cu moves mainly into the 2c site and causes anisotropy increase in lattice constants, leading to relatively low c/a ratios. Cu-containing AB_5 MH alloys with lower c/a ratios were strongly linked to the cycling pulverization rate, which may aggravate the stress concentration and intensify the volume swelling during hydriding/dehydriding cycles [29]. As a result, tailoring the appropriate amount of Cu-substitution is important to the pulverization rates during cycling [30].

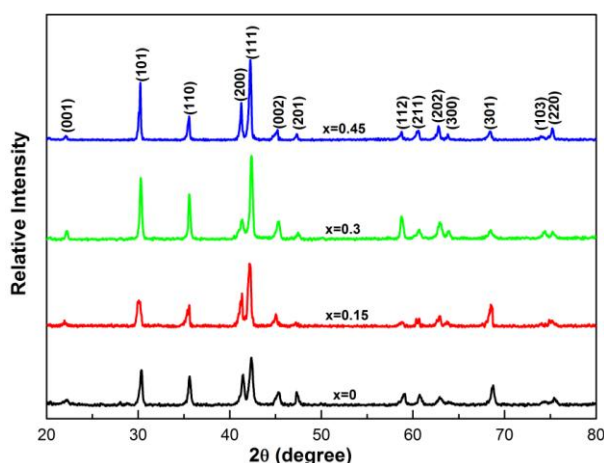


Figure 1. XRD spectra of $\text{LaNi}_{4.1-x}\text{Co}_{0.6}\text{Mn}_{0.3}\text{Cu}_x$ ($x=0-0.45$) hydrogen storage alloys.

Table 1. Lattice parameters of $\text{LaNi}_{4.1-x}\text{Mn}_{0.3}\text{Co}_{0.4}\text{Cu}_x$ ($x=0-0.45$) from XRD analysis.

Cu-content (x)	Lattice constants			Unit cell volume (\AA^3)
	a(\AA)	c(\AA)	c/a	
0	5.0285	3.9897	0.7934	87.37
0.15	5.0329	3.9901	0.7928	87.52
0.3	5.0368	3.9904	0.7923	87.67
0.45	5.0512	4.0007	0.7920	88.39

3.2 Gaseous phase study

The earlier report indicates that the gaseous phase hydrogen storage properties were very important for comparing different hydrogen storage alloys, such as the hydride thermodynamics which is related to high-rate capability and low-temperature capacity [14]. In order to investigate the influence of Cu-addition and temperatures on the hydrogen storage properties of the alloys, the P-C isotherms were measured by PCT at 303, 323 and 353K, and shown in Fig.2 (a-c). The gaseous phase properties obtained from the PCT study are summarized in Table 2. As the Cu-content increases, both the maximum and reversible hydrogen storage capacities (ω_{\max} and ω_{re}) at 303K decrease gradually, as

well as at 323K. The increase in Cu-content in the samples results in a reduction of gaseous phase storage capacity. This is the opposite to the prediction based on the expansion of the unit cell [31]. In the case of Mn-substituted AB₅-based alloys, a positive correlation was established between the storage capacity and the unit cell volume [32]. In this study, the reduction in gaseous phase capacity with Cu-substitution may be related to the occupancy site of Cu.

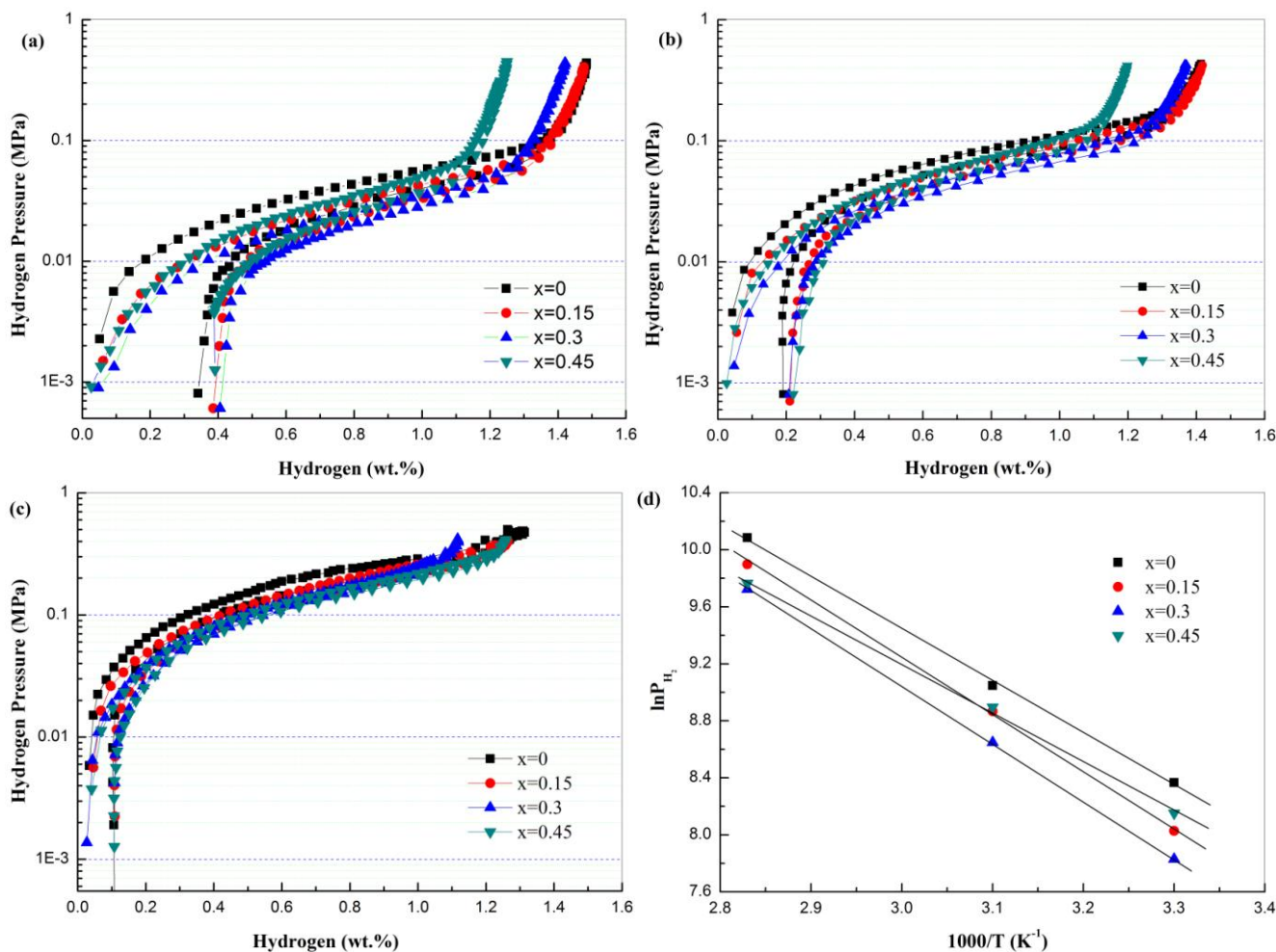


Figure 2. PCT isotherms of LaNi_{4.1-x}Co_{0.6}Mn_{0.3}Cu_x alloys at 303K (a); 323K (b) and 353K (c); and Van't Hoff plots for hydrogen desorption of those alloys (d).

Although the overall unit cell volume increases with Cu-content, the size of the last interstitial site (6m) needed to accommodate hydrogen at the end of absorption may decrease due to the squeezing effect from a Cu atom on the same plane [33].

Compared the ω_{max} and ω_{re} at 303 and 323K, it can be found that the ω_{max} decreases and ω_{re} increases at elevated temperature, resulting in the increase of reversible capacity ratio (RCR) which defined as ω_{re}/ω_{max} . As presented in Table 2, both the RCR at 303 and 323K decrease with increasing Cu-content, and the RCR difference among LaNi_{4.1-x}Co_{0.6}Mn_{0.3}Cu_x (x=0-0.45) gets small gradually with temperature increase. The RCR difference between Cu-free alloy (x=0) and high-Cu alloy

($x=0.45$) is from 0.084 at 303K to 0.05 at 323K, corresponding to reduction of reversible capacity at low temperature. It is attributed to that the desorption equilibrium pressures significantly increase with increasing temperature, which involves the thorough hydrogen desorption from the metal hydride at elevated temperature.

Table 2. Summaries of gaseous phase properties.

Cu-content (x)	Des. Pressure at 303K (MPa)	SF at 303K	PCT hysteresis at 303K	Max. Cap. at 303/323K (wt%)	Rev. Cap. at 303/323K (wt%)	Rev. Cap. Ratio at 303/323K	$-\Delta H$ (kJ/mol)	$-\Delta S$ (J/molK)
0	0.0251	0.925	0.484	1.484/1.413	1.15/1.22	0.772/0.866	30.7	120.44
0.15	0.0208	0.925	0.294	1.477/1.417	1.09/1.21	0.736/0.852	33	125.76
0.3	0.0166	0.926	0.429	1.422/1.371	1.02/1.15	0.715/0.839	33.5	125.67
0.45	0.0161	0.928	0.452	1.25/1.198	0.86/0.98	0.688/0.816	28.43	116.8

Desorption pressure at the mid-point of the desorption isotherm was chosen to represent the equilibrium plateau pressure and listed in Table 2. The general trend of desorption pressure decreases with the Cu-content, indicating a more stable metal hydride with Cu-substitution which corresponds to the enlargement of unit cell. A more stable hydride generally causes a smaller gaseous phase hydrogen storage as reported before on Fe-substituted AB₅-based alloys [23]. Slope factor (SF), defined as the ratio of the storage capacity between 0.01 and 0.1 MPa hydrogen pressure to the total capacity, was used in earlier studies to determine the degree of disorder in the alloys [23], which is related to the absorption/desorption of hydrogen. The Cu-content does not show a large impact on SF since the value of SF increases slightly from 0.925 to 0.928, which indicates that the PCT isotherms became flat with the addition Cu-content.

PCT hysteresis of each alloy is defined as $\ln(P_a/P_d)$, where P_a and P_d are the absorption and desorption equilibrium pressures at the mid-point, respectively. The hysteresis reduces with Cu-content, indicating an increase of the reversibility between hydrogen absorption and desorption that promotes subsequently the hydrogenation and dehydrogenation process [34]. In addition, the hysteresis along with the c/a ratio can predict the pulverization rate of the alloy during cycle [30]. In this case, the c/a ratios and the hysteresis of the Cu-containing alloys are lower than that of the Cu-free alloy, indicating a higher pulverization rate of the low-Cu alloys ($x=0.15$).

The hydride thermodynamics is quite important for comparing different hydrides. The thermodynamic parameters of metal hydrides, enthalpy change (ΔH) and entropy change (ΔS), can be determined from the slope and the intercept of Van't Hoff plot (Fig. 2(d)) based on equation:

$$\ln P = \frac{\Delta H}{RT} + \frac{\Delta S}{R} \quad (1)$$

where R is the gas constant and T is the absolute temperature. The ΔH absolute value is calculated to be 30.7, 33, 33.5 and 28.43 kJ/mol H₂, and ΔS is found to be 120.44, 125.76, 125.67 and 116.8 KJ/mol H₂ corresponding to the LaNi_{4.1-x}Co_{0.6}Mn_{0.3}Cu_x ($x=0-0.45$) alloys, respectively. The ΔH absolute values observed in the endothermic process less than 50 kJ/mol H₂ are close to that of

LaNi₅ (30.6 kJ/mol H₂) [35], indicating the experimental alloys are suitable for electrochemical application as MH negative electrodes [36]. Generally, ΔH is crucial for the thermodynamic stability of metal hydride. A more stable metal hydride with larger ΔH absolute value needs higher temperature to release hydrogen. The more stable Cu-containing alloys having larger ΔH absolute values than that of Cu-free alloy are induced by the expansion of unit cell.

3.3 Electrochemical measurement

Besides the thermodynamics characteristic, both the preactivated process and electrochemical kinetics are also play important roles on the low-temperature capacities, as previous reported that a preactivated process at 303K is necessary for the low temperature properties tests [27]. The discharge characteristics of LaNi_{4.1-x}Co_{0.6}Mn_{0.3}Cu_x (x=0-0.45) alloy electrodes at different temperatures and discharge specific currents is shown in Fig.3 (a), and the electrochemical properties are summarized in Table 3. An apparent variation of discharge capacity has been observed when testing temperature changed from room temperature (activation period) to low temperature (238 K) and discharge current density rose up from 30 mA/g to 60 mA/g. All the alloy electrodes reach their maximum capacity ($C_{\max, 238}$) after 12 cycles at 60mA/g, and show high dischargeabilities above 300 mAh/g even at 238 K, getting to the maximum capacity of commercial AB₅ at room temperature as reported in reference [37]. The superior low-temperature capacities are mainly ascribed to the lower stability of the hydride compared with MmNi₅-type alloy [14]. Noticeably the Cu-contain alloy electrodes exhibit higher dischargeabilities at 238K then at 303K. Chao [38] attributed to the decrease of hydrogen in electrochemical reaction thanks to the release of hydrogen from the alloy electrodes and reduced reversible capacity at elevated temperature. However, as the gaseous phase study, the reversible gaseous phase hydrogen storage capacity reduces at low temperature. Meanwhile, partial equilibrium plateau pressure of the alloys is above 0.1MPa, consequently the reversible self-discharge capacity could not ignored at 303K [39]. Thus the reasonable explain in this cases is that the electrochemical capacity at low temperature is determined by the hydrogen absorption capacity and charge efficiency [40], based on the results of reversible capacity ratio. After additional cycles at low current density, 30 mA/g, the severe pulverization of Cu-contain alloys as predicted above results in more fresh surface area and faster electrochemical kinetics, and consequently the charge efficiency is improved and the higher capacities is obtained at low temperature 238K. Therefore, it is reasonable that the Cu-contain alloys at 238K show higher capacities than at 303K if the alloy electrodes are fully activated with appropriate preactivated process, and the improvement in electrochemical capacity must be essential for improving the charge efficiency at 238K.

Fig. 3(b) shows the dischargecapacities of LaNi_{4.1-x}Co_{0.6}Mn_{0.3}Cu_x alloy electrodes at different discharge specific currents at 238K. With the increasing of discharge currents density, the dischargecapacities decrease accordingly. In details, the capacity of Cu-free alloy (x=0) and Cu-contain alloy (x=0.15) decreases from 320.9 mAh/g and 329.8 mAh/g at 30 mA/g to 63.1 mAh/g and 203 mAh/g at 300 mA/g, respectively. With the addition of Cu, the discharge capacitiesat 238K were

significantly improved at different discharge specific current, and the alloy with $x=0.15$ exhibits the highest discharge capacity at 238K.

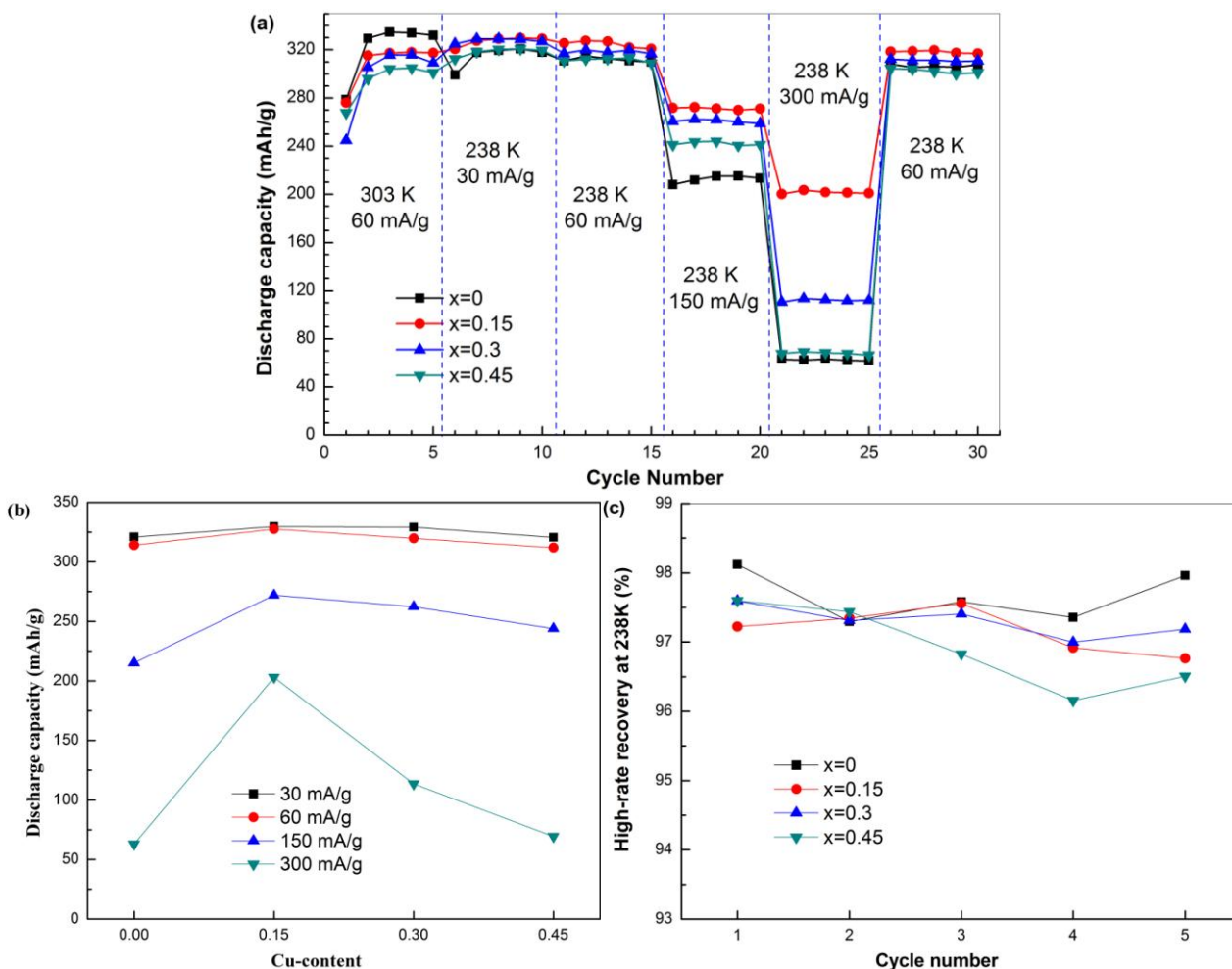


Figure 3. Dischargeability at different temperatures (a), discharge specific currents (b), and HRR_{238} (c) of the alloys.

Table 3. Electrochemical properties of $LaNi_{4.1-x}Co_{0.6}Mn_{0.3}Cu_x$ ($x=0-0.45$) alloy electrodes.

Cu-content (x)	303 K at 60 mA/g			238 K at 60 mA/g		$HRD_{300,T}$ (%)		HRR_{238} (%)
	N_a	C_{max} (mAh /g)	S_{30} (%)	N_a	C_{max} (mAh /g)	303 K	238 K	
0	3	337.8	83.4	12	314.7	98.24	20.08	98.1
0.15	4	318.1	78.5	12	327.6	96.15	61.96	97.2
0.3	4	315.9	82.6	12	319.9	95.17	35.48	97.6
0.45	4	304.9	83.7	12	312	86	22.21	97.6

The isothermal high-rate dischargeability (HRD_T) is an important index, which can be expressed by the following expression:

$$HRD_T(\%) = \frac{C_{300,T}}{C_{60,T}} \times 100 \quad (2)$$

where $C_{300,T}$, $C_{60,T}$ are the discharge capacity at 300 mA/g and 60 mA/g at the constant temperature T , respectively. It can be found from Table 3 that the HRD_{303} decreases monotonously with the increase of x , indicating that the Cu-substitution is adverse to HRD_{303} properties of the alloy electrode, especially for those with high-Cu content. However, the HRD_{238} of the alloys peaks at a content of $x=0.15$, i.e. it firstly increases from 22.08 to 60.96%, then decreases to 22.21% at 238K with the Cu-content. Of the series of alloy in this study, $x=0.15$ for $LaNi_{4.1-x}Co_{0.6}Mn_{0.3}Cu_x$ alloy is the best to enhance the low-temperature discharge capacity at 238K. With the reasonable Cu addition, the discharge capacity $C_{60,238}$ and HRD_{238} is superior to $Mm_{0.7}Mg_{0.3}Ni_{2.58}Co_{0.5}Mn_{0.3}Al_{0.12}$ as reported [27], which is attractive for the Ni/MH battery used in rather low temperature.

Generally, the discharge capacity varies obviously with temperature and discharge current [41-42]. The high-temperature recoverability properties affect the cycling life of the battery [43], as well as the high-rate recoverability properties (HRR), which is defined as the discharge retention after cycling at high-rate discharge current. For the practice application of Ni/MH battery, the HRR is also of great importance at certain using temperature and calculated using the following formula:

$$HRR_T(\%) = \frac{C_{R,T}}{C_{max,T}} \times 100 \quad (3)$$

where $C_{max,T}$ denotes the maximum discharge capacity at 60 mA/g before high-rate discharge cycles and $C_{R,T}$ represents the discharge capacity at 60 mA/g after high-rate discharge cycles at certain testing temperature. It can be seen from Fig. 3(c) that the HRR_{238} for all of the four alloys is above 97% at first, and then hover on a relatively stable value at 238K. It means that the electrodes alloys have suffered few irreversible damage from high-rate discharge cycles. Moreover, as shown in Table 3, the HRR_{238} of Cu-free alloy is higher than those of Cu-contain alloys, implying that the Cu-free alloy is good for the improvement of the anticorrosion property at low temperature.

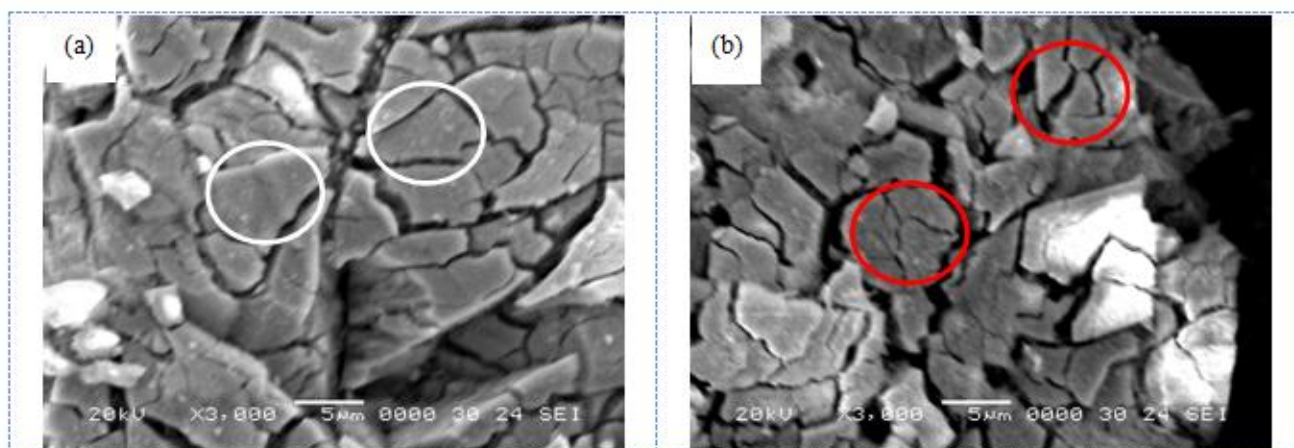


Figure 4. SEM images of $LaNi_{4.1-x}Co_{0.6}Mn_{0.3}Cu_x$ alloy particles after 30 cycles at 303K: (a) $x=0$; (a) $x=0.15$.

Liu [44] attributed the serious capacity degradation of rare-earth based alloy electrodes at initial cycling stage to the pulverization of particles other than oxidation/corrosion of active components. In order to illustrate the pulverization rate, the cycling stability at initial cycling stage, expressed as the following expression:

$$S_{30}(\%) = \frac{C_{30}}{C_{\max}} \times 100 \quad (4)$$

where C_{30} is the discharge capacity at the 30th cycle, and C_{\max} is the maximum discharge capacity at 60 mA/g at 303K, is presented in Table 2. After 30 cycles at 303K, the cycling stability varies from 83.4% ($x=0$) to 78.5% ($x=0.15$), then to 83.7% ($x=0.45$), accordingly it is confirmed that the low-Cu alloys ($x=0.15$) exhibit high pulverization rate as predicted above. In order to verify the pulverization difference, the scanning electron microscopy (SEM) observation of the electrodes after 30th cycles is presented in fig.4. All the bigger particles pulverize to similar average sizes about 2-10 μm . However, many micro-cracks produced in the big particles during the charge/discharge cycle in $x=0.15$ as shown in fig.4(b), which is more obvious than that of $x=0$ as shown in fig. 4(a). Thus the alloy $x=0.15$ exhibits high cycling pulverization rate. As mentioned above, the increase in Cu content lowers the c/a ratios which enlarging the cycling pulverization rate. On the other hand, the increase in Cu content reduces the micro-hardness of the alloys, which improving the pulverization resistance. Therefore, it is reasonable to assume that, the increase in pulverization rate of alloy electrodes with x from 0 to 0.15 is mainly attributed to the former. However, when x exceeds 0.15, the later will become dominant and decrease the pulverization rate. Although all the alloys exhibit a poor cycling stability at 303 K, the degradation of $\text{LaNi}_{4.1-x}\text{Co}_{0.6}\text{Mn}_{0.3}\text{Cu}_x$ are no more than 0.1% per cycle at 238K, which indicates the four alloys is suitable for using at low temperature condition.

3.4 Electrochemical kinetics

In order to clarify the reason of improvement in charge efficiency at relatively low temperatures, the electrocatalytic activity for charge-transfer reaction and hydrogen diffusion in the bulk was evaluated at various temperatures with electrochemical measurements. Fig.5 (a), (b) are the Nyquist plots of the $\text{LaNi}_{4.1-x}\text{Co}_{0.6}\text{Mn}_{0.3}\text{Cu}_x$ ($x=0-0.45$) electrodes at 50% *DOD* after an activation at 303 K and 238K, respectively. A small and large depressed semicircle can be distinguished respectively at the high-frequency and middle-frequency region, and a straight line, which is related to diffusional process, in the low frequency region. The small semicircle represents the contact resistance between the alloy powder and the conductive material, and the large semicircle is related to the charge-transfer resistance on the alloy electrode surface [45]. As can be seen in Fig. 5(a) and (b), the contact impedance remains almost unchanged at both temperatures. The diameter of the semicircle in the middle frequency region decreases firstly with the doping of Cu ($x=0.15$), then increases at both 303K and 238K, similar to the trends of R_{ct} . The R_{ct} of the alloys at 238K are almost one order of magnitude higher than at 303K, indicating a serious polarization at low temperatures.

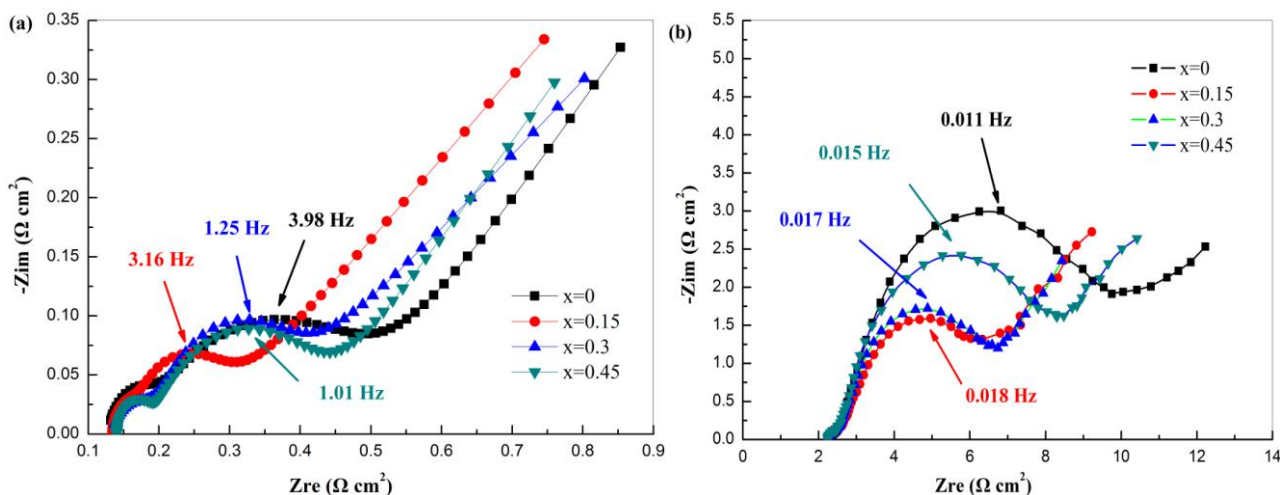


Figure 5. Nyquist plots of LaNi_{4.1-x}Co_{0.6}Mn_{0.3}Cu_x (x=0-0.45) alloy electrodes at 50% SOC after fully activation: (a) EIS at 303K; (b) EIS at 238K.

The exchange current density (I_0) is used to characterize electrochemical activity for charge-transfer reaction on the surface of alloy electrode. Fig. 6(a) shows linear polarization curves of LaNi_{4.1-x}Co_{0.6}Mn_{0.3}Cu_x (x=0-0.45) alloy electrodes. Polarization resistance R_p can be obtained from Fig. 6(a), and consequent exchange current density I_0 can be calculated according to the equation:

$$I_0 = RT/FR_p \quad (5)$$

where R is the gas constant, T the absolute temperature and F the Faraday constant. The results obtained are listed in Table 4. It can be seen that the R_p value decreases firstly, then increases from $x=0$ to 0.45 at both 303K (solid symbols) and 238K (open symbols), which is in agreement with R_{ct} as EIS study. Consequently, I_0 firstly increases from 396.7 and 36.29 mA/g ($x=0$) to 541.7 and 94.38 mA/g ($x=0.15$), then decreases to 468.4 and 53.25 mA/g ($x=0.45$) at 303K and 238K, respectively. Furthermore, the electrocatalytic activity for the charge-transfer reaction was evaluated at various temperatures, and the apparent activation energy ($\Delta_r H$) is introduced to characterize electrocatalytic activity of alloy electrode, which can be calculated in the Equation [45]:

$$\ln\left(\frac{T}{R_p}\right) = C_0 - \frac{\Delta_r H}{RT} \quad (6)$$

where R_p is the polarization resistance, R the gas constant, T the absolute temperature, C_0 the constant related with the specific surface. As the measured values of R_p at different temperatures T are shown in Fig. 6(b), the apparent activation energy firstly increases from 22 kJ/mol ($x=0$) to 16.12 kJ/mol ($x=0.15$), then increase to 18.86 kJ/mol ($x=0.3$), and 19.94 mol kJ/mol ($x=0.45$). The electrocatalytic activity was improved by the addition of Cu from the viewpoint of activation energy.

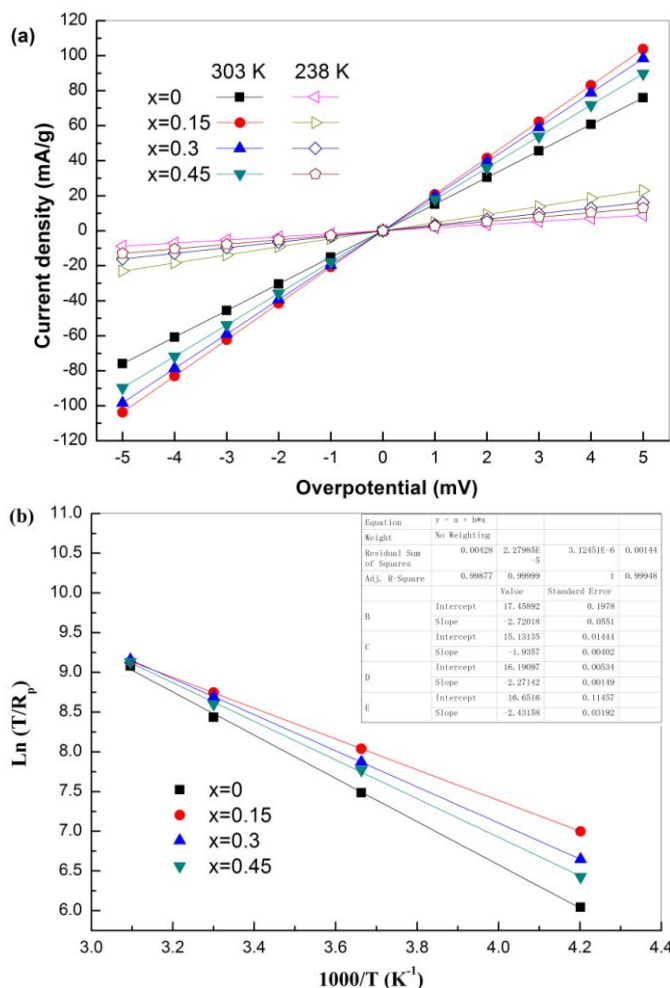


Figure 6. Linear polarization curves (a) and temperature dependence of polarization resistance (b) of LaNi_{4.1-x}Co_{0.6}Mn_{0.3}Cu_x (x=0-0.45) alloy electrodes.

Table 4. Electrochemical kinetics of LaNi_{4.1-x}Co_{0.6}Mn_{0.3}Cu_x (x=0-0.45) alloy electrodes.

Cu-content (x)	R _p (mΩ)		I ₀ (mA/g)		Δ _r H (KJ/mol)	D _H (cm ² /s)		ΔE (KJ/mol)
	303 K	238 K	303 K	238 K		303 K	238 K	
x=0	65.80	564.97	396.73	36.29	22	2.07×10 ⁻⁸	5.18×10 ⁻⁹	12.76
x=0.15	48.19	217.25	541.71	94.38	16.12	1.52×10 ⁻⁸	4.07×10 ⁻⁹	12.17
x=0.3	50.81	308.97	513.78	66.37	18.86	1.40×10 ⁻⁸	3.38×10 ⁻⁹	13.09
x=0.45	55.73	385.05	468.42	53.25	19.94	1.35×10 ⁻⁸	2.03×10 ⁻⁹	15.54

Hydrogen diffusion coefficient D_H used to characterize the hydrogen diffusion rate in bulk alloy can be determined from potential step experiment as our previously report [26], and the hydrogen diffusion coefficient D_H can be estimated from the slope of the linear section after a long discharge time using the following formula [46]:

$$\log i = \log\left(\frac{6FD}{a^2}(C_0 - C_s)\right) - \frac{\pi^2 D_H}{2.303a^2} t \quad (7)$$

in which i is the diffusion current density, d is the material density, a is the particle average radius, F is the Faraday constant, D_H is the hydrogen diffusion coefficient, C_0 is the initial hydrogen concentration in bulk, C_S is the hydrogen concentration at surface and t is the discharge time. Assuming that the alloy powders have a similar distribution with an average particle radius of 16 μm , the D_H is calculated and listed in Table 4.

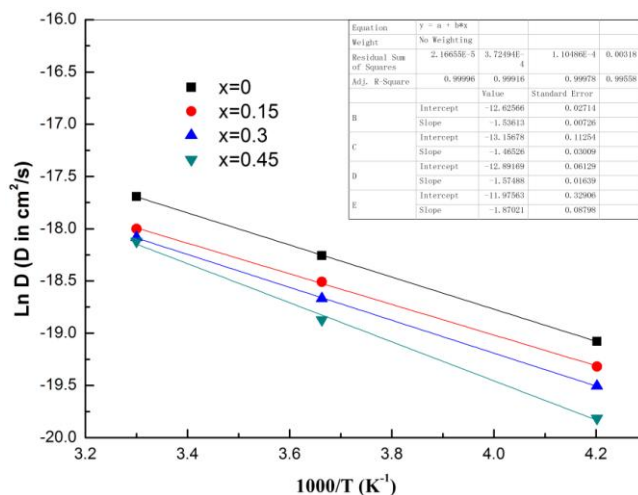


Figure 6. Temperature dependence of hydrogen diffusion coefficient in $\text{LaNi}_{4.1-x}\text{Co}_{0.6}\text{Mn}_{0.3}\text{Cu}_x$ ($x=0-0.45$) metal hydride electrodes.

The D_H decreases monotonously with the Cu-content increase at both temperatures (238 and 303K). The reduction in D_H can be attributed to the additions of Cu, which result in a decrease in c/a ratio and consequently a harder proton hopping in the bulk of the host metal due to the increase of inter-hydrogen distance. This result indicates that the decrease in HRD at 303K with Cu-substitution is due to the lower hydrogen diffusion.

The activation energies for hydrogen diffusion in the four alloys can be calculated in the Equation:

$$\Delta E = -RS \quad (8)$$

where R is the gas constant, S is the slope of $\text{Ln}D_H$ on $1000T^{-1}$, using the Arrhenius equation. Based on the measured values of D_H at different temperatures T (238-303K), the activation energy for hydrogen diffusion firstly increases from 12.76 kJ/mol ($x=0$) to 12.17 kJ/mol ($x=0.15$), then increase to 13.09 kJ/mol ($x=0.3$), and 15.54 mol kJ/mol ($x=0.45$), which is indeed close to the value for LaY_2Ni_9 alloy, 14.84 kJ/mol [47].

The activation energy of hydrogen diffusion is significantly smaller than that of charge-transfer reaction as described above, the hydrogen diffusion in the bulk is not supposed to influenced appreciably by low temperature. From apparent activation energy for charge-transfer reaction and hydrogen diffusion, it is inferred that the charge-transfer reaction on electrode surface is the rate-determining step in the charge process of the negative electrode at 238K. Therefore, the improvement

in surface reactivity must be essential for improving the charge efficiency, which results in improvement of low-temperatures performance of Cu-containing alloys at 238K.

4. CONCLUSIONS

In this study, the effects of Cu content and temperature on the hydrogen storage properties, including gaseous phase hydrogen storage and electrochemical performance, were overall investigated. The following are the major conclusions of this work.

1) XRD analysis shows that $\text{LaNi}_{4.1-x}\text{Co}_{0.6}\text{Mn}_{0.3}\text{Cu}_x$ ($x=0-0.45$) alloys were single phase with hexagonal CaCu_5 crystal structure. The additional Cu mainly moves into the 2c site and causes anisotropic increase in lattice constants, leading to relatively low c/a ratios.

2) With the incorporation of Cu, both the maximum and reversible hydrogen storage capacity, desorption pressure and PCT hysteresis of those Cu-containing alloy decrease obviously. The maximum hydrogen storage capacities decrease, whereas the reversible hydrogen storage capacities increase at elevated temperature, resulting in the increase of reversible capacity ratio. The enthalpies of the experimental alloys are close to -30.6 kJ/mol H_2 of LaNi_5 compound, indicating the experimental alloys are suitable for electrochemical application as MH electrodes.

3) All the alloy electrodes present high dischargeabilities above 300 mAh/g, and good high-rate recoverability properties at 238 K. The Cu-contain alloy electrodes exhibit higher dischargeabilities at 238K then at 303K, which is attributed to the improvement of the charge efficiency at 238K. Furthermore, the amount of Cu-content $x=0.15$ is recommended for the nickel/metal hydride battery used in rather low temperature from the maximum and high-rate dischargecapacity and catalytic properties of the alloy electrodes at 238K.

4) Both the activation energy for charge-transfer reaction and hydrogen diffusion firstly increases from 22 and 12.76 kJ/mol ($x=0$) to 16.12 and 12.17 kJ/mol ($x=0.15$), then increase to 18.86 and 13.09 kJ/mol ($x=0.3$), and 19.94 and 15.54 mol kJ/mol ($x=0.45$), respectively. The electrocatalytic activity was improved by the addition of Cu, whereas the D_{H} decreases monotonously with the Cu-content increase, which indicates that the decrease in HRD at 303K with Cu-substitution is due to the lower hydrogen diffusion. However, the activation energy of hydrogen diffusion are significantly smaller than that of charge-transfer reaction, which indicating that the rate-determining step in the charge process of the negative electrode at 238K was the charge-transfer reaction on the electrode surface.

ACKNOWLEDGEMENTS

This Project is financially supported by the National Natural Foundations of China (51275272, 51261003), Zhejiang Provincial Natural Science Foundation (LQ13E050014), Scientific research project of Zhejiang province education department (Y201431713), the Natural Foundations of Guangxi Province (2012GXNSFGA060002; 201201ZD009).

References

1. J. Prigent, J. M. Joubert and M. Gupta, *Journal of Alloys and Compounds*, 511 (2012) 95.
2. H. B. Yang, H. Fukunaga, T. Ozaki, T. Iwaki, S. Tanase and T. Sakai, *Journal of Power Sources*, 133 (2004) 286.
3. X. Li, L. Wang, H. Dong, Y. Song and H. Shang, *Journal of Alloys and Compounds*, 510 (2012) 114.
4. J. Ren, Y. Zhang, M. Feng, G. Wang, X. Zhao and X. Wang, *Journal of Rare Earths*, 24 (2006) 574 .
5. J. Ma, H. Pan, C. Chen and Q. Wang, *Journal of Alloys and Compounds*, 343 (2002) 164.
6. Z.-H. Ma, J.-F. Qiu, L.-X. Chen and Y.-Q. Lei, *Journal of Power Sources*, 125 (2004) 267.
7. M. V. Ananth, M. Ganesan, N. G. Renganathan and S. Lakshmi, *International Journal of Hydrogen Energy*, 34 (2009) 356.
8. M. Li, S. M. Han, Y. Li, W. Guan, L. R. Mao and L. Hu, *Electrochimica Acta*, 51 (2006) 5926.
9. P. Gifford, J. Adams, D. Corrigan and S. Venkatesan, *Journal of Power Sources*, 80 (1999) 157.
10. T. B. Atwater, P. J. Cygan and F. C. Leung, *Journal of Power Sources*, 91 (2000) 27.
11. E. John K, *Journal of Power Sources*, 80 (1999) 265.
12. G. Günter, *Journal of Power Sources*, 84 (1999) 275.
13. F. Zhang, Y. Luo, A. Deng, Z. Tang, L. Kang and J. Chen, *Electrochimica Acta*, 52 (2006) 24.
14. H. Ye, B. Xia, W. Wu, K. Du and H. Zhang, *Journal of Power Sources*, 111 (2002) 145.
15. X. B. Zhang, D. Z. Sun, W. Y. Yin, Y. J. Chai and M. S. Zhao, *Electrochimica Acta*, 50 (2005) 1957.
16. W. Zhang, S. Han, J. Hao, Y. Li, T. Bai and J. Zhang, *Electrochimica Acta*, 54 (2009) 1383.
17. Y. Li, D. Han, S. Han, X. Zhu, L. Hu, Z. Zhang and Y. Liu, *International Journal of Hydrogen Energy*, 34 (2009) 1399.
18. S. L. Li, P. Wang, W. Chen, G. Luo, D. M. Chen and K. Yang, *Journal of Alloys and Compounds*, 485 (2009) 867.
19. X. B. Zhang, D. Z. Sun, W. Y. Yin, Y. J. Chai and M. S. Zhao, *Electrochimica Acta*, 50 (2005) 2911.
20. C. Khaldi, S. Boussami, B. B. Rejeb, H. Mathlouthi and J. Lamloumi, *Materials Science and Engineering: B*, 175 (2010) 22.
21. K. Young, T. Ouchi, B. Reichman, J. Koch and M. A. Fetcenko, *Journal of Alloys and Compounds*, 509 (2011) 3995.
22. H. Yang, Y. Chen, M. Tao, C. Wu, J. Shao and G. Deng, *Electrochimica Acta*, 55 (2010) 648.
23. K. Young, T. Ouchi, B. Reichman, J. Koch and M. A. Fetcenko, *Journal of Alloys and Compounds*, 509 (2011) 7611.
24. H. Pan, J. Ma, C. Wang, C. P. Chen and Q. D. Wang, *Electrochimica Acta*, 44 (1999) 3977.
25. K. Young, T. Ouchi, A. Banik, J. Koch, M. A. Fetcenko, L. A. Bendersky, K. Wang and M. Vaudin, *Journal of Alloys and Compounds*, 509 (2011) 4896.
26. P. Lv, Z.-m. Wang, Y. Peng, W.-p. Liu, M.-S. Balogun and H.-y. Zhou, *J Solid State Electrochem*, 18 (2014) 2563.
27. C. Ni, H. Zhou, N. Shi and Z. Wang, *Electrochimica Acta*, 59 (2012) 237.
28. C. Zhang, Y. Liu, X. Zhao, M. Yan and T. Gao, *Computational Materials Science*, 69 (2013) 520.
29. X. Wei, S. Liu, H. Dong, P. Zhang, Y. Liu, J. Zhu and G. Yu, *Electrochimica Acta*, 52 (2007) 2423.
30. K. Young, T. Ouchi, W. Mays, B. Reichman and M. A. Fetcenko, *Journal of Alloys and Compounds*, 480 (2009) 434.
31. D. Endo, K. Sakaki and E. Akiba, *Journal of Alloys and Compounds*, 459 (2008) 215.

32. D. Schur, A. F. Savenko, V. A. Bogolepov, S. Zaginaichenko, Z. A. Matysina, A. Magrez, M. Baibarac and T. N. Veziroğlu, in *Black Sea Energy Resource Development and Hydrogen Energy Problems*, A. Veziroğlu and M. Tsitskishvili Editors, p. 179, Springer Netherlands (2013).
33. K. Young, B. Chao, B. Huang and J. Nei, *Journal of Alloys and Compounds*, 588 (2014) 235.
34. W. Jiang, Z. Lan, W. Wenlou, L. Yixin and J. Guo, *International Journal of Hydrogen Energy*, 35 (2010) 11016.
35. B. Rożdżyńska-Kiełbik, W. Iwasieczko, H. Drulis, V. V. Pavlyuk and H. Bala, *Journal of Alloys and Compounds*, 298 (2000) 237.
36. J. Kleperis, G. Wójcik, A. Czerwinski, J. Skowronski, M. Kopczyk and M. Beltowska Brzezinska, *J Solid State Electrochem*, 5 (2001) 229.
37. X. Peng, B. Liu, Y. Fan, X. Zhu, Q. Peng and Z. Zhang, *Journal of Power Sources*, 240 (2013) 178.
38. C. Dongliang, Z. Chenglin, M. Zhewen, Y. Fei, W. Yucheng, Z. Ding, W. Chaoling and C. Yungui, *International Journal of Hydrogen Energy*, 37 (2012) 12375.
39. G. Y. Shang, S. M. Han, J. S. Hao, Y. Liu, X. L. Zhu, Y. Li and D. Y. Xie, *Journal of Alloys and Compounds*, 493 (2010) 573.
40. H. Senoh, Y. Hara, H. Inoue and C. Iwakura, *Electrochimica Acta*, 46 (2001) 967.
41. Z. M. Wang, P.-J. Tsai, S. L. Ip Chan, H. Y. Zhou and K. S. Lin, *International Journal of Hydrogen Energy*, 35 (2010) 2033.
42. Z. M. Wang, C. Y. V. Li and S. L. I. Chan, *Journal of Alloys and Compounds*, 438 (2007) 298.
43. R. Li, J. Wu, Y. Qi and S. Zhou, *Journal of Alloys and Compounds*, 388 (2005) 138.
44. Y. Liu, Y. Cao, L. Huang, M. Gao and H. Pan, *Journal of Alloys and Compounds*, 509 (2011) 675.
45. N. Kuriyama, T. Sakai, H. Miyamura, I. Uehara, H. Ishikawa and T. Iwasaki, *Journal of Alloys and Compounds*, 202 (1993) 183.
46. G. Zheng, B. N. Popov and R. E. White, *Journal of The Electrochemical Society*, 142 (1995) 2695.
47. Y. Belgacem, C. Khaldi, S. Boussami, J. Lamloumi and H. Mathlouthi, *J Solid State Electrochem*, 18 (2014) 2019.

© 2015 The Authors. Published by ESG (www.electrochemsci.org). This article is an open access article distributed under the terms and conditions of the Creative Commons Attribution license (<http://creativecommons.org/licenses/by/4.0/>).